Asymmetric branching ratio for the dissociation of $HD^+(1s\sigma)$

E. Wells,* B. D. Esry, K. D. Carnes, and I. Ben-Itzhak†
J. R. Macdonald Laboratory, Department of Physics, Cardwell Hall, Kansas State University, Manhattan, Kansas 66506-2604
(Received 6 June 2000; published 7 November 2000)

Single ionization of the HD molecule by fast ion impact is used to populate the vibrational continuum of the HD^+ electronic ground state ($1s\sigma$). The resulting dissociation leads to two final states, the lower $1s\sigma$ state or the first excited $2p\sigma$ state, which is 3.7 meV higher at the separated atom limit due to the finite nuclear mass correction to the Born-Oppenheimer approximation. We find dissociation to the lower $H^+ + D(1s)$ state to be about 7% more likely than to the upper $H(1s) + D^+$ final state. The major experimental difficulty in this measurement is the determination of the H_2 contamination in the HD target. Two different methods of determining this contamination are presented, and the details of the measurement of the relative yields of the final two ground-state dissociation channels are discussed. The experimental results are compared to our coupled channels calculation and to a model based on Meyerhof's approximate formulation.

PACS number(s): 34.50.−s, 34.50.Gb

I. INTRODUCTION

The HD^+ molecular ion is a benchmark system for theorists making structure calculations beyond the Born-Oppenheimer approximation [1–3] since the difference in nuclear mass eliminates the symmetry under the exchange of nuclei found in a homonuclear molecule. The effect of this isotopic difference is that the $D(1s)$ threshold is 3.7 meV lower than the $H(1s)$ threshold at the separated atom limit, producing an avoided crossing of the molecular $1s\sigma$ and $2p\sigma$ states, as shown in Fig. 1. The breakdown of the Born-Oppenheimer approximation in HD^+ has been studied, for example, by Carrington and co-workers using microwave spectroscopy to measure the vibrational-rotational transitions of HD^+ near the dissociation limit [4–10]. Their measurements are in agreement with *ab initio* structure calculations only if the calculations include corrections to the Born-Oppenheimer approximation. In addition, by measuring the hyperfine multiplet splitting, Carrington *et al.* [10] showed that the electron is more likely to be located near the deuteron as the vibrational states approach the dissociation limit. Explicitly, they find a large asymmetry in the electron distribution for the $v=21$ level [10], 1.26 meV [11] below the dissociation threshold, but an essentially symmetric distribution for the $v=18$ level, which has a dissociation energy of 74.156 meV [11].

We have recently reported on a similar behavior above the dissociation limit, measuring an asymmetry between the two possible dissociation channels of the ''ground-state dissociation'' (GSD) of $HD^+(1s\sigma)$ [12]. GSD is the dissociation of the HD^+ molecular ion from the vibrational continuum of the electronic ground state ($1s\sigma$). Specifically, we reported that dissociation from $HD^+(1s\sigma)$ to $H^+ + D(1s)$ is about 7% more likely than dissociation into $H(1s) + D^+$. The GSD process is shown schematically in Fig. 1. We initiate GSD using the sudden single ionization of a hydrogen molecule by a fast ion, which preferentially leads to the electronic ground state of the molecular ion. The vast majority of these single ionization events are in vibrationally bound

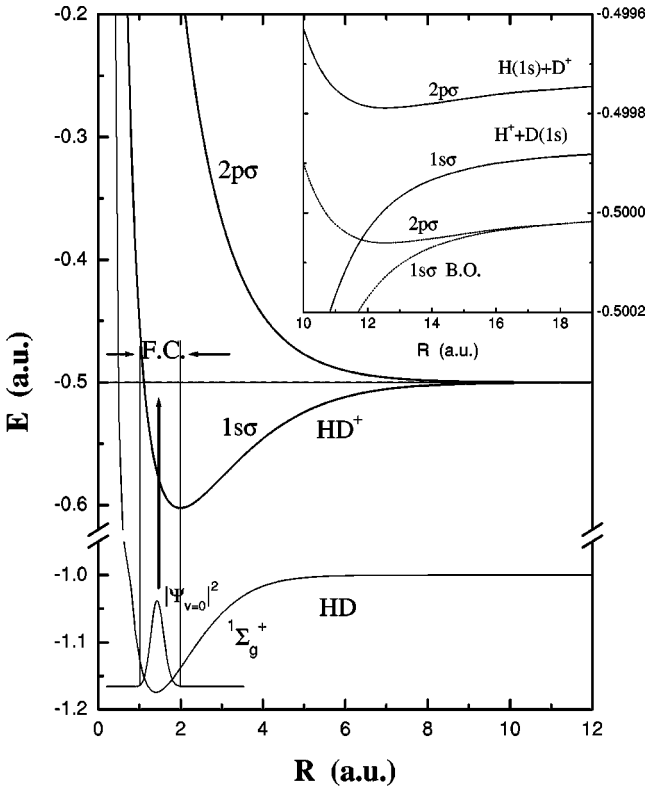

FIG. 1. A schematic view of the GSD process. Sudden ionization of the HD molecule results in vertical transitions to the HD^+ electronic ground state. If the populated $1s\sigma$ vibrational state is in the continuum, a dissociation follows. Charge transfer can then occur near $R=12$ a.u. (shown in the inset) during the dissociation. The potential energy curves are taken from Ref. [22] for HD and from Ref. [1] for HD^+. The inset shows the shift in the $1s\sigma$ and $2p\sigma$ curves from those calculated using the Born-Oppenheimer approximation [25].

*Present address: Department of Physics, University of Virginia, Charlottesville, VA 22904.
†Author to whom correspondence should be addressed. Electronic address: ibi@phys.ksu.edu

states, but about 1% end up in the vibrational continuum and dissociate with a very low kinetic energy, typically less than 1 eV. The population of bound vibrational states and the probability of dissociation as a function of kinetic energy release can be calculated from the Franck-Condon factors that link the neutral and ionic states [13]. Two additional points about the GSD process should be noted. First, since the collision time ($\sim 10^{-17}$ s) is much shorter than the dissociation time ($\sim 10^{-13}$ s), a two-step picture of the process is valid, i.e., first pumping the HD to the vibrational continuum of $HD^+(1s\sigma)$, and then a slower dissociation. Second, by discriminating against the more energetic fragments that result from ionization-excitation and double ionization of the target HD molecule (see Sec. III), we have isolated the events associated with the dissociation of $HD^+(1s\sigma)$.

As the GSD process occurs, there is the possibility of a transition from the initial $1s\sigma$ state to the slightly higher $2p\sigma$ state around the avoided crossing. For a kinetic energy release of less than 3.7 meV, this transition to the $2p\sigma$ state is energetically forbidden. Above that limit, the two states begin to mix, and approach equal probabilities as the kinetic energy release increases. This behavior can be described in a scattering picture as a vertical ionization to the vibrational continuum of the $1s\sigma$ state followed by a possible transition to the first excited $2p\sigma$ state during the dissociation. This process can be expressed as,

$$p + \mathrm{HD} \longrightarrow \underbrace{\mathrm{HD}^+(1s\sigma)} \begin{cases} \longrightarrow \mathrm{H}^+ + \mathrm{D}(1s)\ \text{(elastic scattering)} \\ \longrightarrow \mathrm{H}(1s) + \mathrm{D}^+\ \text{(charge transfer)}, \end{cases} \tag{1}$$

where the lower $H^+ + D(1s)$ final channel is referred to as an ''elastic scattering'' process and the upper $H(1s) + D^+$ final channel is referred to as a ''charge transfer'' process. Within this picture, we have performed coupled channel calculations (described in Sec. II) and compared them to our measurement. This scattering process is different from a typical ion-atom collision in one respect: the range of internuclear distances traversed. In a typical ''full'' collision, the internuclear distance starts and ends at $R=\infty$, while in GSD, the dissociation starts at some finite internuclear distance and increases to $R=\infty$. In this sense, the GSD process can be thought of as ''half'' a collision. In addition to the coupled channel calculations, we have applied a simple model, derived by Meyerhof [14] from the Demkov formulation [15], to the GSD process. Our adaptation of Meyerhof's model is discussed in Sec. II.

There are other processes involving HD^+ in addition to GSD that exhibit isotopic effects, but they are somewhat different in nature. Large isotopic differences have been reported for the collision induced dissociation (CID) of HD^+ molecular ions impinging on atomic and molecular targets at a few keV (see, for example, Refs. [16–19]). It has been shown by Lehman *et al.* [16], that the D^+ fragments are more likely than H^+ fragments by about a factor of 5 following CID of HD^+ at a few keV. They also calculated a similar isotopic preference using a semiclassical theory derived by Rapp [20], which depends strongly on the vibrational excitation. In addition to the preference of D^+ over H^+ in CID, asymmetries between forward and backward scattering along the beam direction have been reported by Dông and Durup [17]. The isotopic preference in CID is much larger and in the opposite direction than the one associated with the GSD process reported here. The difference in isotopic effects is not surprising considering the difference in the excitation mechanisms. In CID, direct vibrational excitation due to energy transfer to the nuclei causes the dissociation of the molecular ion. In contrast, in the GSD process the excitation during the collision is electronic, and the isotopic effect is a result of the mixing between the two lowest coupled molecular states of HD^+ during its very slow dissociation.

Experimentally, measuring the asymmetry between the $1s\sigma$ and $2p\sigma$ final states requires a precise determination of the relative yields of the $H^+ + D(1s)$ and $H(1s) + D^+$ channels. Since the H^+ and D^+ molecular fragments have different masses, they can be separated by their time of flight using an electrostatic extraction field. The measurement of the $H(1s) + D^+$ channel is complicated, however, by the presence of H_2 molecules in the HD target. Single ionization of H_2 by fast ions produces H_2^+ molecular ions, which are difficult to separate from D^+ fragments, since they have the same mass to charge (m/q) ratio.

In this paper we describe the experimental and theoretical techniques that we have used to examine the asymmetry in the dissociation of the electronic ground state of the HD^+ molecular ion. The experimental details are discussed in Sec. III, including two different methods for determining the H_2 contamination. The first involves theoretical knowledge of the ratio of bound-free to bound-bound vertical transitions from HD to HD^+, but allows determination of the H_2 contamination from the time-of-flight measurement alone. This method is described in Sec. III A. The second method, described in Sec. III B, uses two-dimensional momentum imaging to separate the $H_2{}^+$ molecular ions from the D^+ fragments, and thus, allows the direct determination of the H_2 contamination without utilizing theoretical results. The relative merits of each measurement technique are discussed in Sec. IV. Using either method, we are able to empirically demonstrate an asymmetry in the dissociation of the electronic ground state of HD^+. In Sec. II, we briefly present the theoretical methods used: Franck-Condon factors, the coupled channels calculation, and Meyerhof's formula. In Sec. IV we compare the transition probability as a function of collision energy calculated using the approximate analytic formula [14] to our coupled channel calculations. Comparison of the two theoretical results provides a better understanding of when the simple model may be applied, and under what circumstances the more complete calculations must be used to obtain a satisfactory agreement with experiment. Three points are emphasized in this paper. First, we are able to measure the relative yields of the slow H^+ and D^+ fragments precisely enough to demonstrate the symmetry breakdown in GSD, in spite of the difficulties associated with the presence of the H_2 in the target. Second, our experimental

TABLE I. The GSD fractions for three isotopes of the hydrogen molecule.

Isotope	GSD fraction[a] (%)	GSD fraction[b] (%)
H_2	1.4474 ± 0.0082	1.4687 ± 0.0082
HD	0.9947 ± 0.0008	1.0040 ± 0.0008
D_2	0.5206 ± 0.036	0.5233 ± 0.036

[a]The GSD fraction relative to total single ionization.
[b]The GSD fraction relative to bound-bound transitions.

results are described well by our calculations. Finally, the simple Meyerhof model agrees surprisingly well with the more complete coupled channels calculation over most of the kinetic energy release range.

II. THEORY

The Franck-Condon approximation [21] may be used to link the initial and final vibrational states of a molecular transition when the velocity of the projectile used to ionize the molecule is large (such as 4 MeV protons) compared to the vibrational time scale of the molecule. Since the electronic transition rate depends only very weakly on the internuclear distance, the Franck-Condon approximation is satisfied, and the transition rate is proportional to the square of the overlap integral between the initial and final vibrational states. The adiabatic potential energy curves used in our calculation are those of Esry and Sadeghpour for the HD^+ ion [1] and Kołos *et al*. for the neutral molecule [22]. The calculations of the Franck-Condon overlap integrals, described in Refs. [13,23] are essentially identical to the earlier calculation of Tadjeddine and Parlant [24], although our more recent calculations contain one additional bound vibrational state. The results of our calculations of the GSD fractions are given in Table I. The value for the GSD fraction of HD given in Table I is slightly different than the ones given in Refs. [13,23] since we have used improved potential energy curves for HD^+ [1]. This changed the GSD fraction by 0.01% from our previous calculations [13,23]. In addition, the Franck-Condon factors for the HD isotope were calculated using two channels for the HD^+ bound states and then compared to the results obtained using a single channel. Including the second channel had no significant impact on the total GSD fraction. While the difference between the one and two channel calculations of the Franck-Condon factors to specific bound vibrational states is negligible for low lying vibrational states, the difference is more significant near threshold. The calculated Franck-Condon values are approximately 18% different for the $v=22$ state, but only 3% different for $v=21$ and 0.01% different for the $v=19$ state. For the calculation of the GSD fractions for H_2 and D_2, we have taken potential energy curves of the molecular ions from Ref. [25]. Note that the GSD fractions in Table I are given two ways: as the ratio of bound-free to bound-bound transitions and as the ratio of bound-free to total single ionization. The former definition is sometimes more easily compared to other calculations, while the latter is more useful for the purposes of our experiment. The theoretical predictions for the amount of bound-free

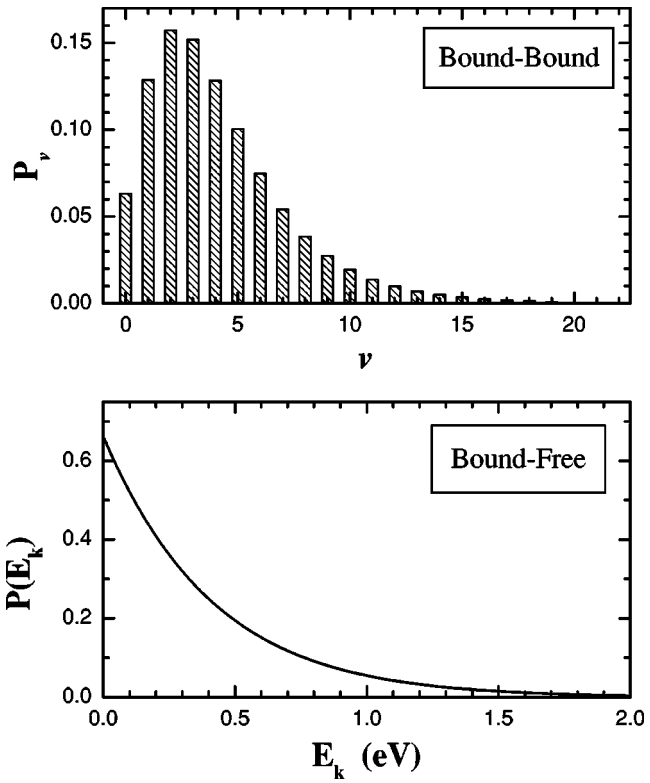

FIG. 2. The transition probability from the HD vibrational ground state to bound vibrational states (top) and the vibrational continuum (bottom) calculated from the Franck-Condon factors. Note that the width of the energy distribution of the bound-free transitions is about 300 meV.

transitions in the D_2 isotope were found to be in good agreement with experiment [13]. Furthermore, the fraction of bound-free out of total single ionization events (about 1% for HD), is sufficiently large to be useful as a production mechanism for studies of very slow $H^+ + D(1s)$ half collisions. Our calculated Franck-Condon factors are shown in Fig. 2 for both bound-bound and bound-free single ionization transitions. Note that the kinetic energy release of the dissociating molecular ion provides half collision energies ranging from $0 \leqslant E_k \leqslant 1.5$ eV.

We have completed calculations of elastic scattering and charge transfer cross sections in these half collisions by solving the two-state coupled channels problem. Using the $1s\sigma$ and $2p\sigma$ adiabatic potentials [1], the coupled channels problem is solved using an *R*-matrix formulation (see, for example, Ref. [26]). A stationary state constructed using the energy-normalized physical incoming wave state has outgoing waves asymptotically only in a single channel [26]. The Franck-Condon transition from the neutral molecule is taken into account by projecting the incoming states onto the ground state of the neutral HD molecule. The coupled channels part of this problem was solved in essentially the same manner used by Esry *et al*. [27] to solve the similar ''full'' collision problem, and the details of the coupled channels calculation may be found there. Our target is cooled to approximately 20 K (see Sec. III), so only $J=0$ is included in the coupled channels calculation since it is the only state

with any significant population at that temperature.

In addition to the coupled channels calculations, we have adopted a model to make quick estimates of the charge transfer probability. The transfer of an electron between the $1s\sigma$ and $2p\sigma$ states of HD^+ during its dissociation is similar to the ''*K*-shell vacancy sharing'' process in fast heavy ion-atom collisions. Creation of a *K*-shell vacancy during a close encounter between a fast heavy ion and an atom followed by the possible transfer of the vacancy to the other collision partner's *K* shell [14,28–30] is an analogous half collision process. The typical energy gap between *K* shells of heavy ions is a few keV, about six orders of magnitude larger than the energy gap in HD^+, which is 3.7 meV. The MeV collision energies in the *K*-shell vacancy sharing experiments (for example, Ref. [31]) are also about a million times larger than the typical kinetic energy release in the GSD process. Hence, scaling the relevant energies in the vacancy sharing process by about a million results in a process similar to GSD. *K*-shell vacancy sharing in fast heavy ion-atom collisions were successfully described within the molecular orbital framework. In particular, Meyerhof [14] derived an analytic expression for the vacancy sharing probability in such collisions. Explicitly, he simplified the more elaborate two-state calculations within the Demkov theoretical treatment [15]. It has been shown by Taulbjerg *et al.* [30] that the formula derived by Meyerhof is a good approximation to their *ab initio* coupled channels calculations of *K*-shell vacancy sharing in fast heavy ion-atom collisions.

Since a basic assumption of the Meyerhof model is a straightline trajectory ($R=v_D t$) [14], deviations from the predicted transition probability are expected at low velocities. We expect, however, that the Meyerhof model might still be applicable in this half collision system even at low collision velocities for two reasons. First, since our target is cool ($T=20$ K), we do not need to be concerned with states having $J>0$. Second, a population of only $J=0$ implies that the dissociation of the HD^+ is colinear, and therefore Meyerhof's assumption of a straightline trajectory is essentially correct.

The probability for electron transfer between the $1s\sigma$ and $2p\sigma$ states, derived by Meyerhof as a vacancy sharing probability [14], is given by

$$w(E_k)=\frac{1}{1+\exp(|2x|)}, \tag{2}$$

where

$$x=\frac{\pi(I_{1s\sigma}-I_{2p\sigma})}{v_D\sqrt{8m_e I}}$$

and $I_{1s\sigma}$ and $I_{2p\sigma}$ are the ionization potentials of the respective states while I is an average value, and v_D is the dissociation speed. Substituting the values for the $H(1s)$ and $D(1s)$ dissociation limits yields for $HD^+(1s\sigma)$ dissociation

$$w(E_k)=\frac{1}{1+\exp(0.01057/\sqrt{E_k})}, \tag{3}$$

where E_k is in atomic units. It is important to note that there is an ambiguity about calculating the relative velocity (v_D) of the two nuclei (or E_k) because of the energy difference between the two dissociation limits (see detailed discussion in Sec. IV).

III. EXPERIMENTAL METHOD

To initiate the GSD process, the target HD molecule is ionized by a fast proton beam which is bunched and accelerated to (usually) 4 MeV by the J.R. Macdonald Laboratory EN Tandem Van de Graaff accelerator, collimated, and directed into the target region. The velocity of the proton beam is high enough that the collision time is much faster than the vibrational time of the HD molecule, and as a result the Franck-Condon approximation is expected to be valid. There are several processes which can create H^+ or D^+ recoil ions during these collisions. Electron capture by the projectile is unlikely at these collision velocities, so dissociative capture processes are not a concern. Since all the vertically excited electronic states of the hydrogen molecule are dissociative, ionization of one electron and excitation of the other yields $H^+ + D(nl)$ or $H(nl) + D^+$. Double ionization of HD results in a $H^+ + D^+$ ion-pair event. Finally, there is the GSD process that is of interest in this study. The proton beam is chosen because it produces less ionization excitation and double ionization of the hydrogen molecule than a more highly charged ion at the same collision velocity [32].

Once the collision takes place, a small percentage of the time (about 1%), a GSD process occurs. The goal of the experiment is to measure the relative yield of the two possible dissociation limit, $H^+ + D(1s)$ and $H(1s) + D^+$. These reaction channels are experimentally distinguished from all other channels producing H^+ or D^+ by taking advantage of the different kinetic energy of these fragments. The kinetic energy released upon dissociation in GSD is less than about 1.5 eV (see Fig. 2) while the ionization-excitation channels release at least 5 eV and typically much more [13,33]. Using a weak extraction field to discriminate against high-energy fragments it is possible to separate the GSD channel from the other channels since most of the higher-energy fragments miss the detector entirely, and those that do not are separated by their longer or shorter times-of-flight [13]. By excluding the recoil ions that are the result of the ionization-excitation and double ionization processes, we are assured that the measured fragments originate from a vertical ionization to a well defined initial state, specifically the $HD^+(1s\sigma)$. The dissociation of this vibrational continuum state can then be thought of as a half collision of $H^+ + D(1s)$ at very low velocities. The two final channels can be separated since the measured H^+ and D^+ fragments have different masses. As previously mentioned, the measurement is complicated by the presence of H_2 in the target, resulting in $H_2{}^+$ molecular ions which must be subtracted from the D^+ channel. We have developed two experimental methods [34] to determine the yield of the low energy fragments which differ mainly in the way the H_2 contamination is evaluated. The first method uses a time-of-flight technique. The second method utilizes the momentum imaging of cold target recoil ion momentum

spectroscopy (COLTRIMS) to measure the yield of the fragments. Both methods share many common features which are described below, while details specific to each technique are described later in Secs. III A and III B.

The detection efficiency for all recoil ions must be equal for an accurate measurement of the $H^+ + D(1s)$ to $H(1s) + D^+$ branching ratio. To ensure this was the case in our experiment, we accelerated the recoil ions to an energy above 3 keV just before hitting the front plate of the highly amplifying *Z*-stack microchannel plate recoil ion detector, and set the lower level discrimination (LLD) sufficiently low to accept all recoil ion signals. In addition, we checked that the ratio of He^{2+}/He^+ for 4 MeV proton impact did not depend on the discrimination level and agreed with the measurement of Knudsen *et al.* [35]. To ensure there were no discrimination effects due to recoil ion velocity, we measured the ratio of H^+/H_2O^+ as a function of the LLD setting and the detector voltage, and conducted the measurements well into the region where this ratio was constant.

The recoil ions are identified by their mass to charge ratio using a time-of-flight technique (TOF$\propto\sqrt{m/q}$). A typical time of flight spectrum measured with a weak extraction field is shown in Fig. 3. Under weak extraction field conditions, most of the higher-energy fragments miss the detector, while all of the molecular ions, which typically have thermal energies, are collected. In order for a higher-energy fragment to reach the detector, the molecule must be oriented at the time of the collision in such a way that the resulting fragment has an initial velocity toward (or away from) the recoil detector. These ''fast'' fragments will either have a shorter (or longer) time-of-flight than the low-energy molecular ions or GSD fragments. The fast fragments appear in the spectrum as shoulders around the $m/q=1$ and $m/q=2$ time-of-flight peaks. The low energy fragments of interest in this study are in the narrow center peak of the time-of-flight spectrum (see Fig. 3). The extraction field strength was chosen so that all of the molecular ions and fragments from GSD are collected, but most of the higher energy events from competing processes miss the detector or are separated in time from the low energy ions.

All measurements are carried out under single collision conditions as determined by a standard pressure dependence measurement. When a low extraction field is used, additional care must be taken to keep the target pressure very low, to ensure that no chemical reactions forming H_2D^+ or $HD_2{}^+$ occur before the recoil fragments exit the target cell. If such a reaction were to occur, the H_2D^+ recoil ions would be indistinguishable from the $D_2{}^+$ recoils ions in our time-of-flight spectrum. We verify that no reactions of this type occur by the absence of the $m/q=5$ peak associated with $HD_2{}^+$ formation in the time-of-flight spectrum.

In addition to the H^+, D^+, and HD^+ recoil ions of interest in our studies, one can see in Fig. 3 contributions from water molecules and H_2 and D_2 contaminants from the HD bottle. The residual water vapor in the vacuum system contributes H^+ and $H_2{}^+$ fragments to the H^+ and D^+ peaks of interest, respectively, and thus it needs to be subtracted. To subtract this contribution, two measurements, with and without the HD target, are conducted, and then the background

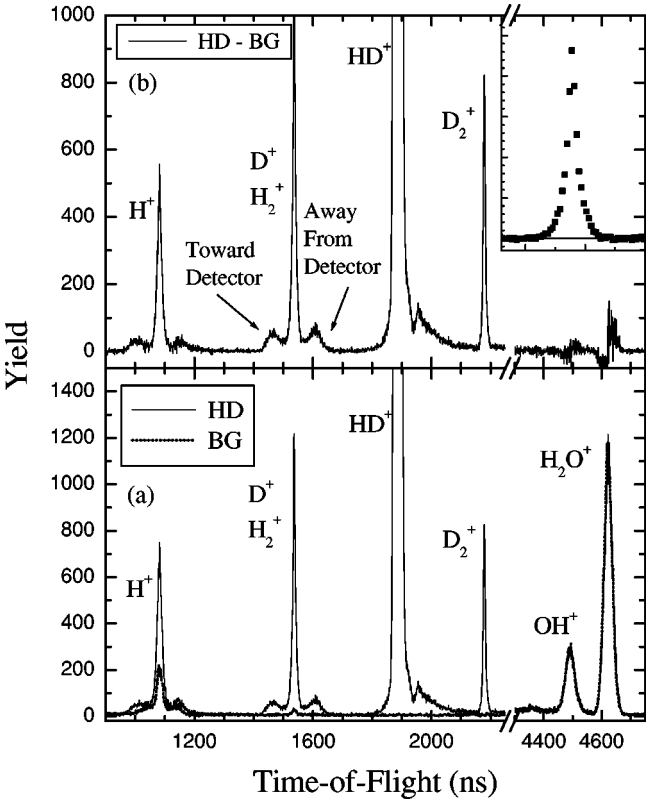

FIG. 3. A typical time-of-flight spectrum of single recoil ions produced by 4 MeV proton impact and measured with a weak (47 V/cm) extraction field. The time-of-flight spectrometer used to obtain this spectrum [23] is somewhat shorter than the one shown in Fig. 4. The shoulders on the H^+ and D^+ peaks are produced by higher-energy fragments from ionization-excitation and double ionization events with an initial velocity towards (or away from) the recoil ion detector. (a) HD target and background (b) HD after background subtraction. The inset shows the $m/q=2$ peak after the baseline and background subtractions. Note the $H_2{}^+$ channel still overlaps with the D^+ channel.

contribution is subtracted after proper normalization of the area of the H_2O^+ peaks in both spectra. Since the two measurements are made under identical conditions, all contributions from the residual water are removed from the $m/q=1$ and $m/q=2$ peaks, where the H^+ and $H_2{}^+$ fragments from water overlap the H^+ and D^+ fragments from HD. The H^+ fragments of water are the major source of uncertainty in the evaluation of the $m/q=1$ peak, while the $H_2{}^+$ fragments of water are only a minor source of error in the $m/q=2$ peak (especially relative to the H_2 contamination in the HD bottle). The resulting spectrum, after the subtraction of the water background, is shown in Fig. 3(b).

Finally, the major experimental challenge in this study is to determine the amount of H_2 contamination in the HD target gas, since the $H_2{}^+$ fragments that result from single ionization of the H_2 impurity contaminate the D^+ fragmentation channel. It is difficult to obtain a pure bottle of HD because over time the HD gas recombines via $HD+HD \rightarrow H_2+D_2$ until the three isotopes have equal abundances. It could be assumed from detailed balance that the amount of H_2 and D_2 contamination would be the same, but this is only

true if the initial contaminations of H_2 and D_2 are the same at the time the bottle is sealed. The problem of H_2 contamination is not unique to our work (see, for example, Ref. [36]) and must often be overcome when using a HD target. The following two subsections describe two different approaches to measuring the H_2 contamination.

A. Time-of-flight technique

Many details of this technique, especially those related to the determination of the H_2 contamination level in the HD target, are discussed in Ref. [23] and will only be briefly presented here. Recoil ions are produced by collisions in the target cell between the incident proton beam and the thin HD gas target. These recoil ions are extracted and accelerated by the uniform electric fields of a two-stage Wiley-McLaren [37] time-of-flight spectrometer toward a recoil ion detector (a microchannel plate detector with a metal anode). The flight times of the recoil ions produced are measured from start signals generated by the recoil ion detector to stop signals synchronized with the beam bunch. The pressure in the target cell was kept around 0.1 mTorr to ensure no secondary collisions of the recoil ions on their way toward the detector. The timing resolution for the data taken using this method ranges between 1 and 1.5 ns, mainly limited by the width of the proton bunch rather than by signal processing. More details of our apparatus may be found in Refs. [13,32,38,39].

A typical time-of-flight spectrum of single recoil ions produced by 4 MeV proton impact, after subtraction of the water vapor background, is shown in Fig. 3(b). The shoulders on the $m/q=1$ and $m/q=2$ peaks caused by the higher-energy fragments were subtracted by using a second order polynomial to fit the baseline [23]. This baseline has only a small contribution near the peak center since fast fragments that are not shifted in time from the peak center must have a relatively large velocity component parallel to the detector and, for the weak extraction field used, miss the detector altogether. After subtraction of the water background and the baseline of fast fragments, the remaining contributions in the spectrum are either molecular ions (with thermal energies) or low energy fragments resulting from GSD of H_2, HD, or D_2. The low-energy center portions of the peaks are numerically integrated to determine the yield, since the peaks do not have a simple shape and curve fitting introduces a systematic error. The area of the $m/q=3$ and $m/q=4$ peaks, denoted $A(3)$ and $A(4)$, are directly related to the yield of HD^+ and $D_2{}^+$ molecular ions, respectively, as these are the unique contributions with that mass to charge ratio. In contrast, there are a few sources of ions with $m/q=1$ and $m/q=2$, which contribute to $A(1)$ and $A(2)$, as listed below

$$A(1)=[\mathrm{HD}^+(1s\sigma)\rightarrow \mathrm{H}^+]+[\mathrm{H_2}^+(1s\sigma)\rightarrow \mathrm{H}^+] \tag{4}$$

and

$$A(2)=[\mathrm{HD}^+(1s\sigma)\rightarrow \mathrm{D}^+]+[\mathrm{D_2}^+(1s\sigma)\rightarrow \mathrm{D}^+]+[\mathrm{H_2}^+], \tag{5}$$

where $[\mathrm{HD}^+(1s\sigma)\rightarrow \mathrm{H}^+]$ and $[\mathrm{HD}^+(1s\sigma)\rightarrow \mathrm{D}^+]$ denote H^+ and D^+ fragments from GSD of HD^+, $[\mathrm{H_2}^+(1s\sigma)\rightarrow \mathrm{H}^+]$ and $[\mathrm{D_2}^+(1s\sigma)\rightarrow \mathrm{D}^+]$ represent H^+ and D^+ fragments from GSD of $H_2{}^+$ and $D_2{}^+$ contaminants, respectively, while the $[\mathrm{H_2}^+]$ is the direct ionization of the H_2 contaminant. It is clear that if a pure HD target could be used then the two dissociation channels of interest, namely, $\mathrm{HD}^+(1s\sigma)\rightarrow \mathrm{H}^+ + \mathrm{D}(1s)$ and $\mathrm{HD}^+(1s\sigma)\rightarrow \mathrm{H}(1s)+\mathrm{D}^+$, would be determined from the respective measurement of $A(1)$ and $A(2)$. Unfortunately such a pure HD target is not available and one has to determine the contributions from the H_2 and D_2 contaminants.

The ground-state dissociation fractions for the hydrogen isotopes of interest are known theoretically from the calculation of the Franck-Condon factors [13,23] given in Table I. For these values we use the notation

$$F^{\mathrm{GSD}}(\mathrm{H_2}^+)=\frac{[\mathrm{H_2}^+(1s\sigma)\rightarrow \mathrm{H}^+]}{[\mathrm{H_2}^+]},$$

$$F^{\mathrm{GSD}}(\mathrm{HD}^+)=\frac{[\mathrm{HD}^+(1s\sigma)\rightarrow \mathrm{H}^+]+[\mathrm{HD}^+(1s\sigma)\rightarrow \mathrm{D}^+]}{[\mathrm{HD}^+]}, \tag{6}$$

$$F^{\mathrm{GSD}}(\mathrm{D_2}^+)=\frac{[\mathrm{D_2}^+(1s\sigma)\rightarrow \mathrm{D}^+]}{[\mathrm{D_2}^+]}.$$

These fractions can be given as the ratio of bound-free to bound-bound transitions from the ground state of the neutral parent molecule as defined above, or as the ratio of bound-free to the total transition to the electronic ground state of the molecular ion (i.e., the sum of bound-free and bound-bound). For convenience both these values are given in Table I. Thus, we just need to know the relative fraction of H_2 and D_2 in the mostly HD target to evaluate the quantities of interest.

The $D_2{}^+$ to HD^+ ratio is easily evaluated as follows:

$$\frac{[\mathrm{D_2}^+]}{[\mathrm{HD}^+]}=\frac{A(4)}{A(3)}. \tag{7}$$

Note that to evaluate the ratio of neutral D_2 to HD a small correction is needed since the amounts of GSD from D_2 and HD isotopes are different [13,23], as shown in Table I.

In contrast, evaluating the $H_2{}^+$ to HD^+ ratio is not an easy task. One way to approach this problem is to take advantage of the theoretical prediction for the GSD of HD^+. Explicitly, we use the fact that the sum $[\mathrm{HD}^+(1s\sigma)\rightarrow \mathrm{H}^+]+[\mathrm{HD}^+(1s\sigma)\rightarrow \mathrm{D}^+]$ is known even though the branching ratio between the two dissociation channels is not. To evaluate the contaminant $H_2{}^+$, we therefore impose a constraint on the sum of the H^+ and D^+ GSD fragments [23]. Adding Eqs. (4) and (5) and dividing by $A(3)$ yields

$$\frac{A(1)+A(2)}{A(3)}=F^{\mathrm{GSD}}(\mathrm{HD}^+)+F^{\mathrm{GSD}}(\mathrm{D_2}^+)\frac{A(4)}{A(3)} +[1+F^{\mathrm{GSD}}(\mathrm{H_2}^+)]\frac{[\mathrm{H_2}^+]}{A(3)}. \tag{8}$$

Solving for $[H_2^+]$ results in

$$\frac{[H_2^+]}{[HD^+]} = \frac{1}{[1+F^{GSD}(H_2^+)]}\left[\frac{A(1)+A(2)}{A(3)} - F^{GSD}(HD^+) - F^{GSD}(D_2^+)\frac{A(4)}{A(3)}\right]. \quad (9)$$

In Eq. (9) the $A(i)$ are the areas evaluated experimentally from the time-of-flight spectrum while the remaining GSD terms come from the calculated Franck-Condon factors (Table I). As with D_2, to evaluate the ratio of neutral H_2 to HD a small correction is needed since the amounts of GSD from H_2 and HD isotopes are different [23].

The D_2 contamination level is always determined with better precision, typically to less than $\pm 1\%$ compared to about $\pm 5\%$ for H_2. Having determined the H_2^+ and D_2^+ contamination levels, Eqs. (4) and (5) can be used to determine the branching ratio for the HD^+ GSD channels. While the determination of the H_2 contamination level depends on the calculation of the GSD fractions, it is important to note that the measurement of the branching ratio of the two HD^+ dissociation channels does not. The evaluation of the $H(1s)+D^+$ dissociation channel is the less accurate of the two dissociation channels because of the H_2^+ contamination present in that channel. In addition, the H_2^+ contamination was determined using the sum $A(1)+A(2)$, so the two dissociation channels are not evaluated independently. Thus, in Sec. IV, when using this method to determine the H_2 contamination, we compare only the measured $H^+ + D(1s)$ dissociation channel to theory.

B. Momentum imaging technique

This technique uses a COLTRIMS-style apparatus to directly measure the H_2 contamination level by means of two-dimensional momentum imaging. The advantage of this technique is that the H_2 contamination can be evaluated independently of any calculations, and the $H^+ + D(1s)$ and $H(1s)+D^+$ dissociation channels can be evaluated independently from Eqs. (4) and (5), respectively. In addition, since the measurements of the two dissociation channels are independent, the sum of the two channels can be used to test the validity of the GSD calculations for the HD^+ isotope in Refs. [13,23].

Over the last decade or so the COLTRIMS technique has proven to be a powerful experimental tool, and the basic apparatus design has been modified in many ways to fit the requirements of different experiments. A discussion of these developments can be found in the topical review by Ullrich *et al.* [40] as well as more recent papers by Abdallah *et al.* [41,42]. The design of our apparatus evolved from two main considerations: First, we wanted to measure the momentum of the low energy recoil ions that result from the GSD process with high precision. In order to do this, the target must be localized and cooled, and the velocity of the recoil ions must be measured. Using COLTRIMS techniques one can measure the momentum of low-energy recoil ions (or electrons) with high precision, since lowering the extraction voltage spreads the distribution out over the detector. Second, we could not afford to expend large amounts of the rather costly HD gas. This eliminated the possibility of using a two- or three-stage supersonic jet typically used in modern COLTRIMS apparatus.

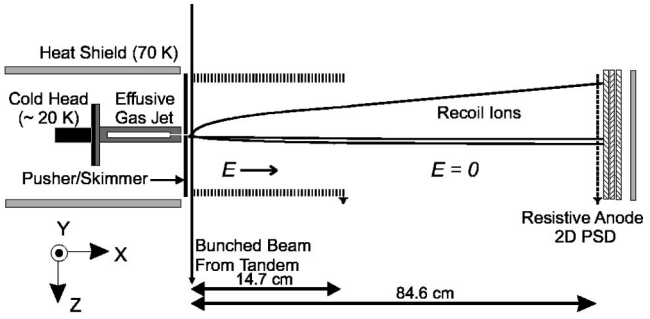

FIG. 4. Conceptual figure of the cylindrically symmetric COLTRIMS-style apparatus used in the momentum-imaging determination of the H_2 contamination.

Our solution was to build a precooled effusive jet to localize the target, extract the ions with a spectrometer that included a weak electrostatic lens for spatial focusing of the ions, and measure the position of the recoil ions with a two-dimensional resistive anode position sensitive detector. This approach, while not a COLTRIMS apparatus by the strict definition of the term [41], since we do not measure the momentum of all the charged fragments that are a result of the collision, retained many of the advantages of COLTRIMS while the gas consumption of the effusive jet was small enough to be economically feasible. A conceptual view of our apparatus is shown in Fig. 4. A small gas cell is mounted on the cold head of a cryopump. The HD gas flows into this cell and is cooled to approximately 20 K by collisions with the cell walls. A heat shield at liquid nitrogen temperature surrounds most of the cold head and gas cell, limiting radiative heating of the gas cell by the rest of the apparatus, which is at room temperature. An effusive jet of the precooled gas traveling toward the recoil ion detector is formed when the gas escapes out of a 0.36 mm diameter hole at one end of the cylindrical gas cell. The gas pressure in the cell is kept low enough that molecular flow conditions are valid. The length to width ratio of the tube is about 9:1, therefore, the resulting effusive jet gives a somewhat directional flow [43], which further cools the target gas in the transverse direction. The effusive jet is further collimated by a 1 mm diameter hole in the pusher plate of the spectrometer. The resulting target is about 1.5 mm in diameter in the collision region (about 2 to 3 mm from the pusher plate) where it intersects the fast proton beam which has been collimated to about 0.5×0.5 mm.

The recoil ions are extracted and accelerated by the electric fields of the spectrometer. The spectrometer consists of 31 ($63.5\times 63.5\times 1$ mm) brass plates separated by ceramic spacers. The first plate (the pusher/skimmer) has a 1 mm hole in the center to allow gas flow from the effusive jet. The other 30 plates have a 57 mm diameter hole in the middle. The distance from the front of one plate to the front of an

adjacent plate is 5.6 mm. 980 kΩ resistors connect each adjacent pair of plates. Spatial focusing of the target is accomplished by applying voltage to the pusher and one other spectrometer electrode (the focus electrode, plate number 11, where the pusher/skimmer is plate number 1). This creates two uniform potential gradients on either side of the focus, and since there is no grid at the focus electrode, the change in the electric field from one region to the next forms an electrostatic lens, a common COLTRIMS technique to improve momentum resolution [34,44–46]. Once the ions leave the spectrometer, they travel through a 662 mm drift region. A 200 lines/inch electroform mesh is placed 5.5 mm in front of the first microchannel plate of the recoil ion detector, which operates at approximately -2.4 kV. The mesh is needed so the high voltage applied to the front of the microchannel plates does not produce fields that distort the field free drift region. The spatial focusing of the spectrometer was checked using SIMION [47]. This focusing results in an effective target size comparable to the position resolution of the detector.

The time of flight of the recoil ions was measured in much the same way as in the time-of-flight technique (see Sec. III A). The start signal for the timing is taken from the rear of the last channel plate of the *Z*-stack microchannel plate detector, because this signal has a much faster rise time than the signal from the resistive anode. Once again, a signal synchronized with the bunched proton beam was used as a stop.

A spectrometer with a single uniform extraction field has first order focusing in the time-of-flight direction if the drift region is twice as long as the acceleration region. Due to the lens used for spatial focusing in our spectrometer, a longer drift region is required for time focusing. Our detector position was chosen for the best combination of focusing in all three spatial dimensions. The long drift region, in combination with the relatively weak extraction fields used, results in recoil ion flight times of at least several μs. The repetition rate of the proton bunch was typically 21.2 μs. In practice, the timing resolution is limited by the width of the proton bunch, which was approximately 1–2 ns for the data reported here. The electronic resolution of the system is slightly above 1 ns, mainly because we use a 1 ns time-to-digital-converter (TDC) to record the time of flight. Furthermore, even though the spectrometer can achieve good focusing in all three spatial dimensions, for the purpose of determining the H_2^+ contamination, we were primarily interested in the information in the *y* and *z* directions, and as a result, slightly favored spatial focusing over time focusing when choosing the focus voltage for this experiment. The two-dimensional resistive anode recoil ion detector used has a position resolution of 0.18 mm/channel. Factoring in the thermal distribution of the target gas, for the extraction field used in this measurement ($\sim$14 V/cm in the collision region) the momentum resolution in the *y* and *z* directions is approximately 0.7 a.u.

As in the time-of-flight technique described in Sec III A, the identity of the ions was determined by their time of flight, and much of the same analysis of the yields of the low energy H^+ and D^+ fragments was made. In contrast, however, the H_2 contamination was determined from the measured two-dimensional momentum distributions. A prediction of the energy distribution of the $m/q=2$ peak is shown in Fig. 5, assuming equal amounts of H_2^+ and $H(1s)+D^+$. If a Maxwell-Boltzmann distribution is assumed for the molecular ions, and they are sufficiently cold (note the different distributions for 30 and 300 K in Fig. 5) then the GSD contribution and the H_2 contamination should be separable by their energy, or equivalently, their momentum. Consider the distributions of momentum perpendicular to the extraction field shown in Fig. 6. This data was taken using a very low extraction field (12.5 V/cm at the collision region). The sharp peak in the middle of the $m/q=2$ momentum distribution, shown in Fig. 6(a), is the molecular ions resulting from single ionization of the H_2 contamination. Those H_2^+ molecular ions, since they were measured at the same time as the HD^+ molecular ions shown in Fig. 6(b), should have a similar shape as that ''pure'' molecular ion peak, since they each have the same thermal distribution. The difference in mass of the molecular ions, however, does mean that the H_2^+ momentum distribution is slightly narrower, since

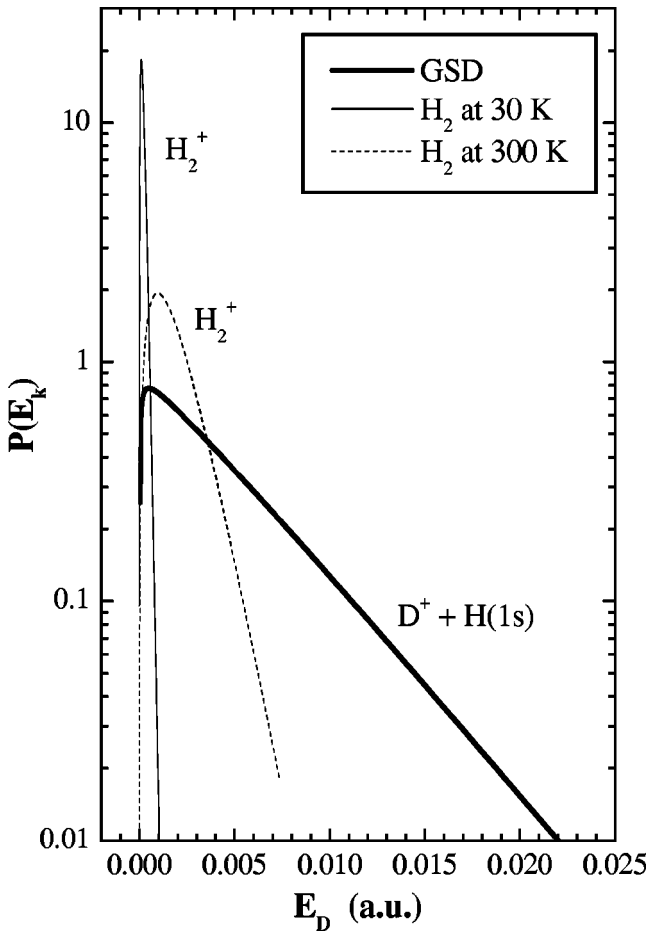

FIG. 5. Prediction of $m/q=2$ energy distributions assuming a Maxwell-Boltzmann distribution for the H_2^+ molecular ions and the Meyerhof model convoluted with the Franck-Condon overlap integrals for the $H(1s)+D^+$ dissociation channel (assuming equal populations). The population of H_2^+ as a function of energy is shown for 30 and 300 K.

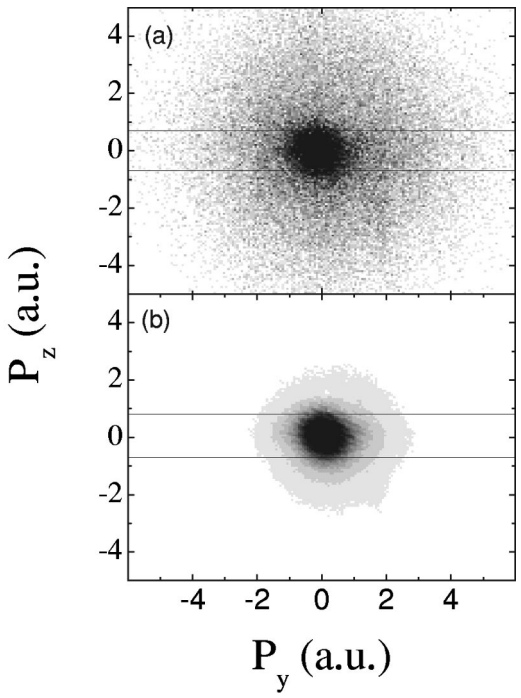

FIG. 6. (a) Perpendicular momentum distributions for $m/q=2$. The $m/q=2$ distribution contains both a narrow distribution of H_2^+ molecular ions and a wider distribution of low energy D^+ fragments from GSD. (b) Perpendicular momentum distributions for $m/q=3$, which contains only a narrow distribution of HD^+ molecular ions. The lines mark the slices shown in Fig. 8.

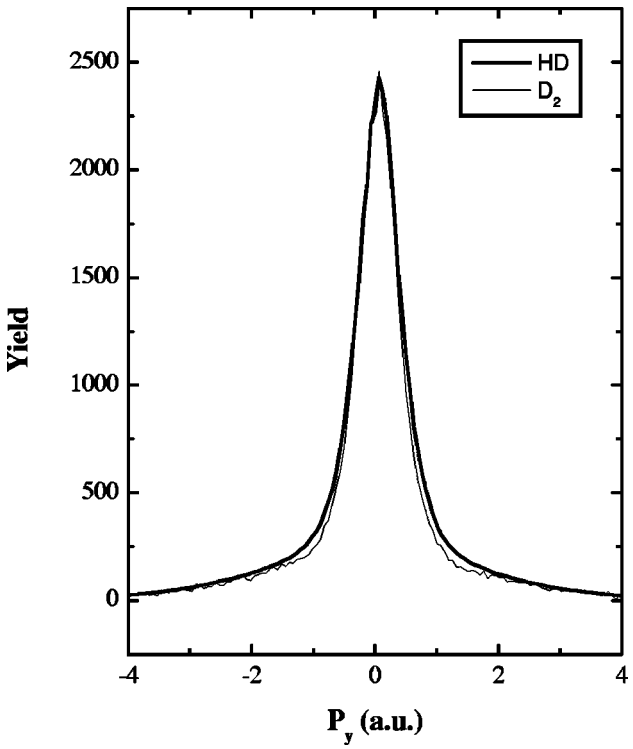

FIG. 7. A comparison of the P_y momentum distributions of HD^+ and D_2^+. The HD^+ distribution has been scaled according to Eq. (10).

$$\frac{P_{H_2^+}}{P_{HD^+}} = \sqrt{\frac{m_{H_2^+}}{m_{HD^+}}}. \tag{10}$$

The D^+ fragments in the $m/q=2$ peak, on the other hand, have a wide momentum distribution due to the kinetic energy released upon dissociation, as well as a minimum at $P=0$ due to the threshold behavior. The two components of the $m/q=2$ distribution, a narrow peak of H_2^+ molecular ions and a wide distribution of D^+ fragments from GSD, can easily be seen in Fig. 6(a).

To evaluate the H_2^+ fraction relative to the dominant HD^+ channel, we first scale the perpendicular momentum of the HD^+ by the factor given in Eq. (10) on an event-by-event basis in order to produce the expected momentum distributions for H_2^+. To verify that such scaling of the momentum of HD^+ peak is correct, we have also performed the same scaling on the D_2^+ peak. Figure 7 shows that the scaled one-dimensional P_y momentum distributions of HD^+ and D_2^+ match nicely. Projecting a narrow vertical slice around $P_z=0$ out of the momentum distributions shown in Fig. 6 onto the P_y axis accomplishes two things: First, it reduces somewhat the contribution from collisions that occurred outside the jet along the beam direction (sometimes referred to as a ''hot gas'' contribution). Second, the slice is chosen so essentially the entire H_2^+ (or D_2^+ for Fig. 7) contribution is included in the slice, but only a small percentage of the GSD events appear in the slice. An identical slice is taken out of the HD^+ distribution. Since the middle of the two projections have the same shape, determining the H_2 contamination is just a matter of normalizing the HD^+ peak so it matches the H_2^+ peak. Since the shape of the peak is determined experimentally, scaling by Eq. (10) leaves only one free parameter for our fit, the number of H_2^+ molecular ions relative to the number of HD^+ molecular ions. A comparison between the H_2^+ peak and the scaled HD^+ peak is shown in Fig. 8. The $m/q=2$ distribution contains also D^+ fragments in the background, so only the center portion of the projection is matched. Subtracting the scaled HD^+ peak from the H_2^+ peak leaves only the contribution from the D^+ peak, which is expected to have a minimum near $P_y=0$. This minimum is the indicator that determines the scaling factor for the amplitude of the HD^+ peak. Too large of a contamination fraction gives a minimum value significantly less than zero. Too small of a contamination fraction does not produce a satisfactory minimum. We define the average of these two values as the best fit, and the difference between the ''too large'' and ''too small'' gives the uncertainty in the fit. A few values for the H_2 contamination illustrating the ''fitting'' procedure are shown in Fig. 9.

Determining the H_2 contamination level by this method eliminates the need to use the theoretical value for the GSD fraction of HD^+ in Eq. (9) to determine the H_2 contamination and enables the determination of the yields of the two dissociation channels, $H^+ + D(1s)$ and $H(1s) + D^+$, from Eqs. (4) and (5), respectively. In order to get enough resolution to make the best fit of the H_2 contamination, the extraction field must be lowered to a value for which many of the fragments from GSD miss the detector. To evaluate the total

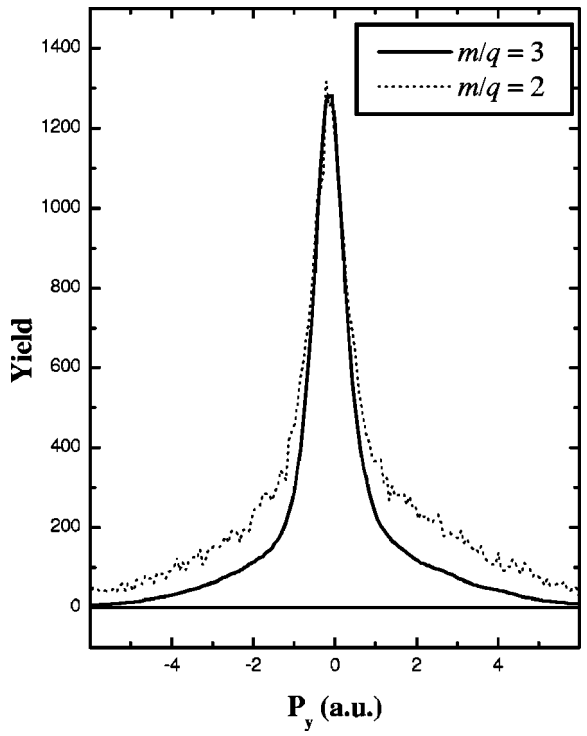

FIG. 8. The projected slices (marked by the lines on Fig. 6) of the $m/q=2$ and $m/q=3$ momentum distributions. The momentum of the HD^+ distribution has been scaled according to Eq. (10) and in amplitude to determine the amount of H_2 contamination.

yield of the GSD fragments, the extraction field must be raised to a value where all of the GSD fragments are collected, but, as in the first method, most of the fragments from the ionization-excitation or double ionization either miss the detector or are shifted in time from the molecular ions and GSD fragments. From the time-of-flight spectrum taken with this higher extraction field (94 V/cm at the collision region) $A(1)$, $A(2)$, $A(3)$, and $A(4)$ are evaluated as discussed in Sec. III A, and the yield of both the $H^+ + D(1s)$ and $H(1s) + D^+$ channels are then evaluated directly from Eqs. (4) and (5). Only the H_2 contamination is determined with the lower extraction field.

IV. RESULTS AND DISCUSSION

When applying the higher extraction field to the spectrometer (sufficient to collect all of the GSD fragments), the momentum imaging apparatus described in Sec. III B collects the same information as our previous time-of-flight spectrometer described in Sec. III A. In that case, we can evaluate the H_2 contamination using only the time-of-flight, or we can reduce the extraction field to measure the H_2 contamination using two-dimensional momentum imaging. In this manner, we have measured the H_2 contamination in two HD bottles using both methods to determine if the two methods yield consistent results. For the first bottle, the ratio of $H_2{}^+$ to HD^+ was determined to be $0.53 \pm 0.02\%$ using the time-of-flight technique. Using the momentum imaging technique on the same bottle, the ratio was measured as $0.510 \pm 0.015\%$. More recently, we have determined the H_2 contamination in a second bottle to be $0.420 \pm 0.02\%$ using the momentum imaging technique and $0.410 \pm 0.025\%$ using the time-of-flight technique. These results are consistent with each other, showing that either of the two methods may be used to determine the H_2 contamination level. The major advantage of the momentum imaging technique is that it allows the yield of the H^+ and D^+ fragments from GSD to be measured independently as the determination of the H_2 contamination does not rely on any theoretical calculations. The increase in the error for the second bottle is a result of using 20 MeV C^{3+} ions to produce the vertical ionization transitions to the vibrational continuum of $HD^+(1s\sigma)$ instead of the more favorable fast protons. The ratio of ionization-excitation to single ionization (and the ratio of double to single ionization) is larger for C^{3+} than for the fast protons we typically use Refs. [13,32,39] and the increased error bar reflects the increased uncertainty in the subtraction of these competing processes. For comparison, the measured D_2 contamination was $0.477 \pm 0.002\%$ in the first bottle and $0.472 \pm 0.003\%$ in the second bottle. The D_2 contamination is de-

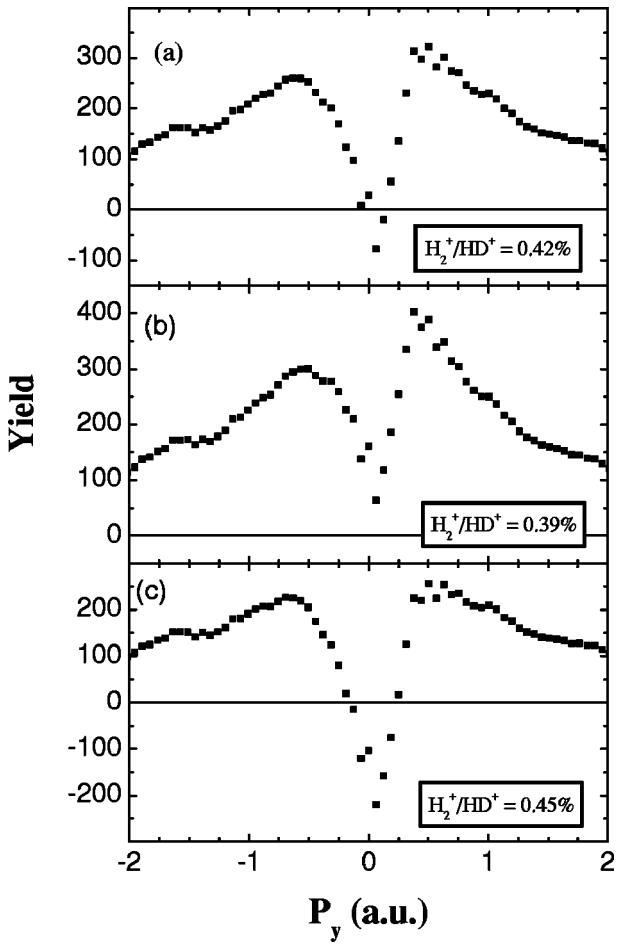

FIG. 9. The difference between the $m/q=2$ and HD^+ P_y momentum slice. (a) shows the average of these two values, which we designate the best fit for this particular data. In (b), the estimate of $H_2{}^+/HD^+$ is too small, and a significant number of D^+ events still remain at $P_y=0$. In (c), on the other hand, too much has been subtracted, and the resulting minimum in the momentum slice is too wide.

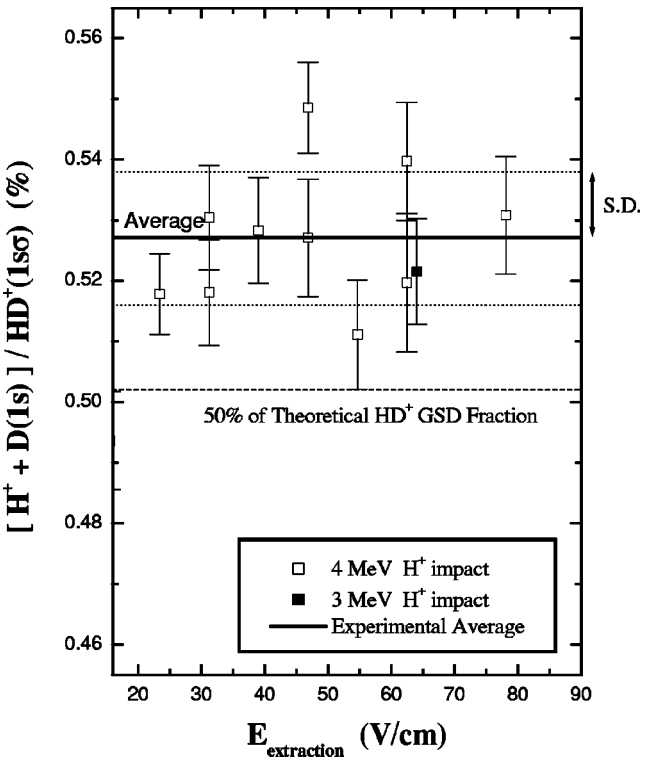

FIG. 10. The yield of $H^+ + D(1s)$ relative to $HD^+(1s\sigma)$ measured with the time-of-flight technique as a function of extraction field. The dotted lines above and below the average value represent one standard deviation from the average result. The dashed line is the expected value for a symmetrical branching ratio. The measured values are significantly different from a symmetric dissociation.

termined more precisely than the H_2, since it is the only recoil ion with $m/q=4$.

Using the time-of-flight technique the yield of H^+ GSD fragments is measured relative to the HD^+ yield. Our results are shown in Fig. 10 as a function of the extraction field on the spectrometer. The extraction field is varied to diminish the possibility of systematic errors related to ion impact energy and spot size on the detector. Since this method requires the application of the constraint that the sum of the H^+ and D^+ fragments must add up to the total GSD fraction for HD in order to determine the $H_2{}^+$ contamination, we can independently measure only one of the GSD channels. Having our choice, we choose the $H^+ + D(1s)$ channel, since the $H_2{}^+$ contamination plays only a minor role in the evaluation of this channel, and consequently the uncertainty is smaller than with the $H(1s) + D^+$ channel. In Fig. 10 we compare the results of the time-of-flight technique to the expected ratio of H^+/HD^+ if a symmetric dissociation is assumed, that is, an equal population of the $1s\sigma$ and $2p\sigma$ final states. The average measured value of H^+/HD^+ is 0.527% and the standard deviation is 0.011%. This is significantly different (2.3σ) from the symmetric dissociation value of 0.502%. The experimental results are summarized in Table II. Note that in Table II the experimental data is presented relative to total single ionization, that is, relative to the sum of all of the channels given in Eq. (1).

Using the momentum imaging method to evaluate the H_2 contamination, we can independently measure both dissociation channels, as well as verify that the Franck-Condon overlap integrals give the correct ratio of bound-free transitions to total single ionization events. These results, shown in Table II, are consistent with the results from the time-of-flight technique. Furthermore, the measured yield of the $H(1s) + D^+$ channel agrees with the theoretical values. Ionization of the HD target by 20 MeV C^{3+} projectiles had no significant effect on the process except that the increase in production of recoil ions from double ionization and ionization-excitation of the HD target slightly increased the error bars (see Table II). This is expected, since qualitatively, as long as the ionization mechanism satisfies the Franck-Condon approximation, it should not affect the GSD process. Taken together, the results of our measurements clearly point to a measurable symmetry breakdown in the dissociation of the HD^+ ground electronic state. Thus, the isotopic effect causing the breakdown of the Born-Oppenheimer approximation for HD^+ not only results in the localization of the electron around the deuteron, as demonstrated by Carrington *et al.* [10], but is also responsible for a measurable preference for the $H^+ + D(1s)$ state in the vibrational continuum.

These results might seem, at first glance, to be somewhat

TABLE II. Summary of the experimental results using two different methods, the results obtained from a Meyerhof model, and the theoretical results. The three values for the Meyerhof model are obtained using different values for v_D in Eq. (2) as explained in the text. All of the results are presented relative to total single ionization of HD.

Method	$H^+ + D(1s)$ (%)	$H(1s) + D^+$ (%)	$F^{GSD}(HD^+)$ (%)
Time-of-flight	0.522 ± 0.011		
Momentum Imaging	0.520 ± 0.009	0.483 ± 0.016	1.003 ± 0.018
Momentum Imaging[a]	0.517 ± 0.012	0.473 ± 0.022	0.990 ± 0.025
Coupled channels	0.539	0.455	0.994
Eq. (2)—KER$=E-E_{D(1s)}$	0.534	0.460	
Eq. (2)—KER[b]$=E-E_{D(1s)}$	0.536	0.458	
Eq. (2)—KER$=E-E_{H(1s)}$	0.529	0.465	

[a]Measured with 20 MeV C^{3+} projectiles instead of 4 MeV protons.
[b]Truncating the probability below the $D(1s)$ threshold.

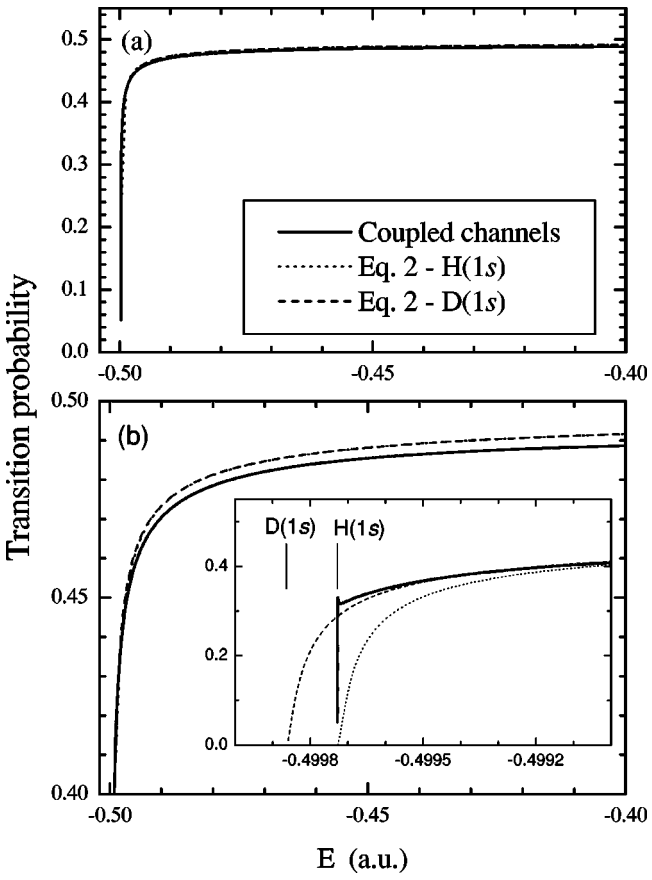

FIG. 11. The transition probability between the $1s\sigma$ and $2p\sigma$ states, $w(E_k)$ (see definition in text), as a function of energy above the D($1s$) dissociation threshold: (a) Overall view, (b) magnified view of the threshold region (inset) and ''high-energy regime.'' The calculations using Meyerhof's formula were conducted twice, with kinetic energy releases relative to the H($1s$) and D($1s$) thresholds (see text).

surprising, given the range of the kinetic energy release in the GSD process (FWHM≈300 meV) [13] compared to the size of the energy gap between the $1s\sigma$ and $2p\sigma$ final states (3.7 meV). Qualitatively, however, it is easier to understand these results when you consider that the distribution of possible kinetic energy release values peaks at zero [13], so the most probable kinetic energy releases are ones where the lower energy $1s\sigma$ state should be favored. More quantitatively, the theoretical $1s\sigma$ to $2p\sigma$ transition probability w is shown in Fig. 11 as a function of the kinetic energy upon dissociation [relative to the H($1s$) threshold]. We have defined w as

$$w(E_k)=\frac{\sigma_{\text{transfer}}(E_k)}{\sigma_{\text{transfer}}(E_k)+\sigma_{\text{elastic}}(E_k)}, \tag{11}$$

rather than the more conventional definition of a transition probability

$$\sigma_{1\to 2}=\frac{|S_{21}|^2}{k_1^2}, \tag{12}$$

since it will be easier to compare Eq. (11) directly to experimental results. This transition probability, w, increases rapidly from zero at threshold and later approaches 0.5 asymptotically for both the coupled channels calculations and Meyerhof's analytic formula, as shown in Fig. 11(a). There is a nice overall agreement between the two. A closer look, however, at these calculated probabilities, shown in Fig. 11(b), reveals some differences. First, Meyerhof's formula overestimates the transition probability at large energies, but only by about 0.7%, not a large inaccuracy ''price'' for the associated gain in simplicity. In contrast, near threshold the disagreement between Meyerhof's formula and the coupled channels calculations is significant, as shown in the inset of Fig. 11(b). Not only does Meyerhof's formula fail to describe the threshold behavior properly, it is not clear what threshold one should use to evaluate the relative nuclear speed, v_D, in Eq. (2). In the GSD process, the asymptotic value of v_D is evaluated relative to the lower D($1s$) threshold associated with the initial $1s\sigma$ state. If charge transfer occurs during the dissociation, however, the nuclear speed can no longer be evaluated in the same way, as v_D now becomes relative to the upper H($1s$) threshold. As a result, there is some ambiguity in applying the Meyerhof model at collision energies comparable with the energy gap between the upper and lower states. If one uses the lower D($1s$) threshold the agreement with the coupled channels probability extends to lower energies, but some transitions can occur in the energetically forbidden region. This is avoided if one uses the higher H($1s$) threshold but then Meyerhof's formula under estimates the coupled channels probability significantly and over a wider energy range. It seems that the best way to apply the Meyerhof formula is to use the lower threshold and set the transition probability to zero below the H($1s$) threshold.

The total fraction of GSD which is transferred to the $2p\sigma$ final state, which is the measured value in this experiment, is given by $P_{2p\sigma}=\int_0^\infty dE_k P(E_k)w(E_k)$, where $P(E_k)$ is the probability for a kinetic energy release E_k. The value of $P(E_k)$ is given by the Franck-Condon factors for the vibrational continuum [13,23]. The probability for GSD remaining on the initial $1s\sigma$ state is given by $P_{1s\sigma}=\int_0^\infty dE_k P(E_k) - P_{2p\sigma}=\int_0^\infty dE_k P(E_k)[1-w(E_k)]$. The computed values using the different versions of the Meyerhof formula discussed above are given in Table II. It can be seen that the integrated value using the kinetic energy release relative to the H($1s$) threshold fits the coupled channels calculation best, because of the cancellation of the underestimate at low energies with the overestimate at high energies. Furthermore, using this threshold prevents transitions in the energy forbidden region below the H($1s$) threshold. However, as can be seen from Fig. 11(b), this probability fails more in describing the transfer probability just above threshold. If one uses the truncated probability which best approximates the behavior near threshold, the deviation of the integrated value is minimal, much smaller than our experimental errors in the measurement of the total transition probability.

V. SUMMARY

We have presented the results of experimental studies of the dissociation of the electronic ground state of HD^+ fol-

lowing vertical single ionization of HD by fast ion impact. The $H^+ + D(1s)$ dissociation channel is about 7% more likely than the $H(1s) + D^+$ dissociation channel. This demonstrates that the asymmetry in the electron distribution, previously measured in high bound vibrational states of HD^+ [10], extends above the dissociation threshold. The major experimental difficulty in this measurement was the determination of the amount of H_2 in the HD target. Two different methods, one depending on theoretical knowledge of the GSD fractions, and one a direct measurement, were used to determine this contamination with consistent results. Our experimental results are in agreement with both a simple model based on the Meyerhof formula for vacancy sharing and a fully quantum mechanical coupled channels calculation. The Meyerhof model seems to match the coupled channels results fairly well if the relative nuclear velocity is determined from the lower threshold and the transition probability is set to zero below the $H(1s)$ threshold. A more stringent test of the theory could be provided by a measurement of the transition probability as a function of the kinetic energy release. Improvements in our momentum imaging experimental technique should allow this. The GSD process results in a $H^+ + D(1s)$ half collision with some collision energies much smaller than those that have been measured with merged beams [48], thereby opening new possibilities for empirical examination of this near-resonant charge transfer process. The major challenge in such an experiment would be the accurate determination of the kinetic energy release of each GSD event.

ACKNOWLEDGMENTS

The authors would like to thank C.L. Cocke and A.L. Landers for helpful advice in the development of the COLTRIMS-like experimental method, and O.L. Weaver, Vidhya Krishnamurthi, and H.R. Sadeghpour for many useful discussions. This work was supported by the Chemical Sciences, Geosciences and Biosciences Division, Office of Basic Energy Sciences, Office of Science, U.S. Department of Energy and by a National Science Foundation grant to the Institute for Theoretical Atomic and Molecular Physics at the Harvard-Smithsonian Center for Astrophysics.

[1] B. D. Esry and H. R. Sadeghpour, Phys. Rev. A **60**, 3604 (1999).
[2] R. E. Moss and I. A. Sadler, Mol. Phys. **61**, 905 (1987).
[3] J. Macek and K. A. Jerjian, Phys. Rev. A **33**, 233 (1986).
[4] A. Carrington, Science **274**, 1327 (1996).
[5] A. Carrington and J. Buttenshaw, Mol. Phys. **44**, 267 (1981).
[6] A. Carrington, J. Buttenshaw, and R. A. Kennedy, Mol. Phys. **48**, 775 (1983).
[7] A. Carrington and R. A. Kennedy, Mol. Phys. **56**, 775 (1985).
[8] A. Carrington, I. R. McNab, and C. A. Montgomerie, Mol. Phys. **64**, 679 (1988); **64**, 983 (1988); **65**, 751 (1988).
[9] A. Carrington, I. R. McNab, C. A. Montgomerie, and J. M. Brown, Mol. Phys. **66**, 1279 (1989).
[10] A. Carrington, I. R. McNab, C. A. Montgomerie-Leach, and R. A. Kennedy, Mol. Phys. **72**, 735 (1991).
[11] G. G. Balint-Kurti, R. E. Moss, I. A. Sadler, and M. Shapiro, Phys. Rev. A **41**, 4913 (1990).
[12] I. Ben-Itzhak, E. Wells, K. D. Carnes, Vidhya Krishnamurthi, O. L. Weaver, and B. D. Esry, Phys. Rev. Lett. **85**, 58 (2000).
[13] I. Ben-Itzhak, Vidhya Krishnamurthi, K. D. Carnes, H. Aliabadi, H. Knudsen, U. Mikkelsen, and B. D. Esry, J. Phys. B **29**, L21 (1996).
[14] W. E. Meyerhof, Phys. Rev. Lett. **31**, 1341 (1973).
[15] Yu. N. Demkov, Sov. Phys. JETP **18**, 138 (1964).
[16] T. A. Lehman, J. R. Hass, F. W. Crow, K. B. Tomer, and L. G. Pedersen, Int. J. Mass. Spectrom. Ion Processes **66**, 85 (1986).
[17] P. Dông and J. Durup, Chem. Phys. Lett. **5**, 340 (1970).
[18] R. W. Rozett and W. S. Koski, J. Chem. Phys. **49**, 2691 (1968).
[19] S. E. Kupriianov and V. K. Potapov, Sov. Phys. JETP **33**, 311 (1957).
[20] D. Rapp, J. Chem. Phys. **32**, 735 (1960).
[21] E. U. Condon, Phys. Rev. **32**, 858 (1928).
[22] W. Kolos, K. Szalewicz, and H. J. Monkhorst, J. Chem. Phys. **84**, 3278 (1986).
[23] I. Ben-Itzhak, E. Wells, Vidhya Krishnamurthi, K. D. Carnes, H. Aliabadi, U. Mikkelsen, O. L. Weaver, and B. D. Esry, Nucl. Instrum. Methods Phys. Res. B **129**, 117 (1997).
[24] M. Tadjeddine and G. Parlant, Mol. Phys. **33**, 1797 (1977).
[25] Z. Chen, Ph.D. thesis, Kansas State University, 1991 (unpublished), and private communication.
[26] M. Aymar, C. H. Greene, and E. Luc-Koenig, Rev. Mod. Phys. **68**, 1015 (1996).
[27] B. D. Esry, H. R. Sadeghpour, E. Wells, and I. Ben-Itzhak, J. Phys. B (to be published).
[28] U. Fano and W. Lichten, Phys. Rev. Lett. **14**, 627 (1965).
[29] M. Barat and W. Lichten, Phys. Rev. A **6**, 211 (1972).
[30] K. Taulbjerg, J. Vaaben, and B. Fastrup, Phys. Rev. A **12**, 2325 (1975).
[31] H. Kubo, F. C. Jundt, and K. H. Purser, Phys. Rev. Lett. **31**, 647 (1973).
[32] E. Wells, I. Ben-Itzhak, K. D. Carnes, and Vidhya Krishnamurthi, Phys. Rev. A **60**, 3734 (1999).
[33] A. K. Edwards, R. M. Wood, J. L. Davis, and R. L. Ezell, Phys. Rev. A **42**, 1367 (1990).
[34] E. Wells, Ph.D. thesis, Kansas State University, 2000 (unpublished).
[35] H. Knudsen, L. H. Andersen, P. Hvelplund, G. Astner, H. Cederquist, H. Danard, L. Liljeby, and K.-G. Rensfelt, J. Phys. B **17**, 3545 (1984).
[36] B. Sheehy, B. Walker, and L. F. DiMauro, Phys. Rev. Lett. **74**, 4799 (1995).
[37] W. C. Wiley and I. H. McLaren, Rev. Sci. Instrum. **26**, 1150 (1955).
[38] I. Ben-Itzhak, S. G. Ginther, and K. D. Carnes, Nucl. Instrum. Methods Phys. Res. B **66**, 401 (1992).
[39] I. Ben-Itzhak, Vidhya Krishnamurthi, K. D. Carnes, H. Aliabadi, H. Knudsen, and U. Mikkelsen, Nucl. Instrum. Methods Phys. Res. B **99**, 104 (1995).

[40] J. Ullrich, R. Moshammer, R. Dörner, O. Jagutzki, V. Mergel, H. Schmidt-Böcking, and L. Spielberger, J. Phys. B **30**, 2917 (1997).

[41] M. A. Abdallah, M. Achler, H. Bräuning, A. Bräuning-Deminiam, C. L. Cocke, A. Czasch, R. Dörner, A. L. Landers, V. Mergal, T. Osipov, H. Schmidt-Böcking, M. J. Singh, T. Weber, W. Wolff, and H. E. Wolff, in *Proceedings of the 18th International Conference on X-Ray and Inner Shell Processes*, Chicago, 1999, edited by R. Dunford, D. S. Gemmell, E. P. Kanter, B. Krössig, S. H. Southworth, and L. Young (AIP, College Park, MD, 2000), pp. 101.

[42] M. A. Abdallah, A. Landers, M. Singh, W. Wolff, H. E. Wolf, E. Y. Kamber, M. Stöckli, and C. L. Cocke, Nucl. Instrum. Methods Phys. Res. B **154**, 73 (1999).

[43] H. Pauly in *Atomic and Molecular Beam Methods*, edited by Giacinto Scoles (Oxford University Press, New York, 1988), Vol. 1, pp. 87–92.

[44] R. Dörner, H. Bräuning, J. M. Feagin, V. Mergel, O. Jagutzki, L. Spielberger, T. Vogt, H. Khemliche, M. H. Prior, J. Ullrich, C. L. Cocke, and H. Schmidt-Böcking, Phys. Rev. A **57**, 1074 (1995).

[45] V. Mergel, *Dynamische Elektron Korrelation in Helium* (Shaker Verlag, Aachen, 1996).

[46] A. L. Landers, Ph.D. thesis, Kansas State University, 1999 (unpublished).

[47] D. A. Dahl, SIMION 3D Version 6.0, Lockheed Martin Idaho Technologies, Idaho National Engineering Laboratory, 1995.

[48] J. H. Newman, J. D. Cogan, D. I. Zeigler, D. E. Nitz, R. D. Rundel, K. A. Smith, and R. F. Stebbings, Phys. Rev. A **25**, 2976 (1982).